Received: 14 March 2023 | Revised: 17 July 2023 | Accepted: 8 August 2023

DOI: 10.1002/hbm.26464

RESEARCH ARTICLE

WILEY

Lifespan neurodegeneration of the human brain in multiple sclerosis

Pierrick Coupé[1] | Vincent Planche[2,3] | Boris Mansencal[1] | Reda A. Kamroui[1] | Ismail Koubiyr[4,5] | José V. Manjòn[6] | Thomas Tourdias[4,5]

[1]CNRS, Univ. Bordeaux, Bordeaux INP, LABRI, Talence, France

[2]Univ. Bordeaux, CNRS, Bordeaux, France

[3]Centre Mémoire Ressources Recherches, Pôle de Neurosciences Cliniques, CHU de Bordeaux, Bordeaux, France

[4]Inserm U1215 - Neurocentre Magendie, Bordeaux, France

[5]Service de Neuroimagerie diagnostique et thérapeutique, CHU de Bordeaux, Bordeaux, France

[6]Instituto de Aplicaciones de las Tecnologías de la Información y de las Comunicaciones Avanzadas (ITACA), Universitat Politècnica de València, Valencia, Spain

Correspondence
Pierrick Coupé, Domaine universitaire, 351, cours de la Libération, 33405 Talence, France.
Email: pierrick.coupe@labri.fr

Funding information
French National Research Agency, Grant/Award Number: ANR-18-CE45-0013; Laboratory of Excellence TRAIL, Grant/Award Number: ANR-10-LABX-57; IdEx Bordeaux, Grant/Award Number: ANR-10-IDEX-03-02; French Ministry of Education and Research; Centre national de la recherche scientifique; Spanish Ministerio de Ciencia e Innovación, Grant/Award Number: PID2020-118608RB-I00; University of Bordeaux's France 2030 program / RRI "IMPACT"

Abstract

Atrophy related to multiple sclerosis (MS) has been found at the early stages of the disease. However, the archetype dynamic trajectories of the neurodegenerative process, even prior to clinical diagnosis, remain unknown. We modeled the volumetric trajectories of brain structures across the entire lifespan using 40,944 subjects (38,295 healthy controls and 2649 MS patients). Then, we estimated the chronological progression of MS by assessing the divergence of lifespan trajectories between normal brain charts and MS brain charts. Chronologically, the first affected structure was the thalamus, then the putamen and the pallidum (around 4 years later), followed by the ventral diencephalon (around 7 years after thalamus) and finally the brainstem (around 9 years after thalamus). To a lesser extent, the anterior cingulate gyrus, insular cortex, occipital pole, caudate and hippocampus were impacted. Finally, the precuneus and accumbens nuclei exhibited a limited atrophy pattern. Subcortical atrophy was more pronounced than cortical atrophy. The thalamus was the most impacted structure with a very early divergence in life. Our experiments showed that lifespan models of most impacted structures could be an important tool for future preclinical/prodromal prognosis and monitoring of MS.

KEYWORDS
atrophy, lifespan, MRI, multiple sclerosis, staging, thalamus

1 | INTRODUCTION

Multiple sclerosis (MS) is a chronic, demyelinating and inflammatory pathology of the central nervous system, that involves significant neurodegenerative damages. The brain atrophy resulting from neurodegeneration is an important biomarker of disease progression, even better than the traditional white matter lesion assessment (Filippi et al., 2013).

Magnetic resonance imaging (MRI) has proven to be a useful tool for estimating brain atrophy in neurodegenerative diseases. In MS, MRI mainly focuses on the white matter lesions to establish the initial diagnosis (Thompson et al., 2018) and to monitor therapeutic

response, but MS progression could also be monitored through volumetric measures independently of relapses (Marciniewicz et al., 2019). Thanks to advances in automatic analysis of brain MRI, the volume of brain structures can be estimated accurately and robustly (Coupé et al., 2020a). Therefore, while previously focusing on global brain volume, recent studies have been able to analyze MS-related brain atrophy more finely at the structural level (Eshaghi, Marinescu, et al., 2018).

Evidence suggests that global brain atrophy is mainly driven by gray matter (GM) alterations rather than to white matter damage (Fisher et al., 2008). These GM alterations have been found in both cortical and subcortical structures in MS patients (Amato et al., 2004). Also, some brain structures seem more likely to be affected than others (Eshaghi, Marinescu, et al., 2018). GM atrophy has been observed across all the stages of the disease even in preclinical MS stage (e.g., clinical isolated syndromes—CIS and radiologically isolated syndrome—RIS) (Azevedo et al., 2015; Dalton et al., 2004; Henry et al., 2008; Labiano-Fontcuberta et al., 2016). Moreover, several studies investigated the progression of GM atrophy across MS phenotypes (Eshaghi, Marinescu, et al., 2018). However, so far, we do not know when such a process starts and the full dynamic over several decades has not been revealed. Without a database starting long before the appearance of the first symptoms and providing the corresponding follow-up over decades, such a study is very challenging.

Recently, the concatenation of a large number of cross-sectional data has been used to reveal the typical course of brain volumes during the lifespan (Coupé et al., 2017). We pioneered an approach that consists in comparing such normative trajectories with those from patients, and we demonstrated its relevance to estimate preclinical GM atrophy in Alzheimer's disease (Coupé et al., 2019; Planche et al., 2022) and the three clinical variants of frontotemporal dementia (Planche et al., 2023). To overcome the lack of data prior to clinical diagnosis, pathological lifespan modeling combines healthy subjects and patients covering the entire lifespan. In this study, we propose to adapt this strategy to MS. Thanks to these lifespan models, we present new insights on the spatiotemporal evolution of GM atrophy across the entire lifespan. Moreover, we estimate the most atrophic structures, the sequence of impacted structures and the average age of onset of atrophy.

2 | METHODS

2.1 | Standard protocol approvals, registrations, and patient consents

All the used images were obtained from public datasets. Database providers ensured compliance with ethical guidelines such as informed consent and anonymization (see Acknowledgments).

2.2 | Datasets

In our study, lifespan models of brain volume trajectories were estimated using 24 open-access MRI databases. To this end, we collected MRIs of 41,671 subjects, 38,978 from cognitively normal, healthy control (HC) subjects covering the entire lifespan (from 1 to 100 years of age) and 2693 from patients with MS. All the MRIs were collected on 1.5T or 3T magnets (see Table S1 for details).

2.2.1 | HC database

For HC subjects, we used the baseline T1-weigthed MRI from the following datasets: *UKbiobank* ($n = 29932$), *C-MIND* ($n = 236$), *NDAR* ($n = 382$), *ABIDE* ($n = 492$), *ICBM* ($n = 294$), *IXI* ($n = 549$), *ADNI1&2* ($n = 404$), *AIBL* ($n = 232$), *OASIS* ($n = 298$), *ADHD-200* ($n = 544$), *DLBS* ($n = 315$), *ISYB* ($n = 213$), *MIRIAD* ($n = 23$), *PPMI* ($n = 166$), *PREVENT-AD* ($n = 307$), *Amsterdam open MRI collection* (AOMIC_ID100 & PIOP1 & PIOP2, $n = 1361$), *Calgary cohort* ($n = 267$), *CamCAN* ($n = 653$), *PIXAR* ($n = 155$), *SALD* ($n = 494$), *SRPBS* ($n = 791$), *NACC* ($n = 161$), *NIFD* ($n = 135$) and *SLIM* ($n = 574$). After quality control (QC), this database contained 38,295 HC subjects (see Tables 1 and S1 for more details).

2.2.2 | MS database

For MS patients, we used the first available T1-weighted and FLAIR MRIs from the "Observatoire Français de la Sclérose en Plaques" (OFSEP) dataset ($n = 2692$) including 544 subjects with a clinically isolated syndrome (CIS), 1686 patients with relapsing–remitting multiple sclerosis (RRMS), 288 secondary-progressive multiple sclerosis (SPMS) and 174 patients with primary-progressive multiple sclerosis (PPMS) (Vukusic et al., 2020). After QC, this database contained 2649 MS subjects (see Table 1). The average age at the first of symptoms suggestive of MS was 32 years and the average age at the MRI used for analysis was 42 years. Finally, 65.5% of these patients had disease-modifying therapy (DMT).

2.3 | Construction of lifespan groups

To study the brain volumetric trajectories of HC subjects and MS patients across the entire lifespan, we compiled several open-access databases to construct normal and diseased models. For the HC models, we used the 38,295 MRIs from HC subjects remaining after QC covering the entire lifespan (see Table 1). For the MS models, we followed the strategy proposed in (Coupé et al., 2019; Planche et al., 2022) for lifespan analysis of Alzheimer's disease and frontotemporal dementia (Planche et al., 2023). This framework is based on the assumption that neurodegeneration is a continuous and progressive process along the pathology evaluation. Therefore, to constrain the model over the entire lifespan, it has been proposed to mix HC with patients. Herein, we combined MRIs of 2649 MS patients after QC (see Table 1) with MRIs of 3711 healthy controls younger than 23 years. This age was the quantile at 5% of the MS population that enabled a smooth transition from HC subjects to MS patients. These HC subjects were all the subjects younger than 23 years in the 38,295 HC subjects used for HC models after

TABLE 1 Databases description.

	n	Sex	Age at first symptom mean (years) [range]	Age at MRI mean (years) [range]	EDSS median (years) [range]
HC subjects	38,295	F = 19,025; M = 19,270	n.a	57.5 [0.7–100.2]	n.a
MS patients	2649	F = 1917; M = 732	32.1 [5–73]	42.1 [13.0–79.0]	3.0 [0–9.0]

Note: This table provides the total number (*n*) of considered images (after quality control), the sex proportion, and the average ages and intervals in brackets.

QC. Consequently, for the MS models, between 1 and 13 years only HC subjects were used, between 13 and 23 years a mix of HC subjects and MS patients were used, and after 23 years only MS patients were used. At the end, the parametric MS models were constrained over the entire lifespan using 6360 subjects. To ensure model validity, we analyzed results over 1–62 years, 62 years being the quantile at 95% of the MS population age distribution.

2.4 | Image processing

All the considered T1-weighted MRI were segmented using AssemblyNet (Coupé et al., 2020b) (https://github.com/volBrain/AssemblyNet/). This software produces fine-grained segmentation (i.e., 132 structures) of the entire brain.

2.4.1 | Pipeline for HC subjects

All the T1-weighted MRI were first preprocessed to harmonize them. The preprocessing consisted of denoising (Manjón et al., 2010), inhomogeneity correction (Tustison et al., 2010), affine registration into the Montreal Neurological Institute (MNI) space (Avants et al., 2011), tissue-based intensity normalization (Manjón et al., 2008) and intracranial cavity segmentation (Manjón et al., 2020a). Afterward, all the preprocessed images were checked by automatic quality control (QC) based on artificial intelligence (Denis de Senneville et al., 2020). This QC method has been designed to estimate error of affine registration into MNI space. This step is the main source of error observed during preprocessing. Finally, structure segmentation was achieved with AssemblyNet using 250 deep learning models through a multi-scale framework (Coupé et al., 2020b). AssemblyNet has been intensively validated on several datasets with different acquisition protocols and scanners, as well as on infant, adult and elderly brains with and without pathologies. During this validation, the high robustness and the reproducibility of AssemblyNet were also assessed using scan-rescan experiments.

2.4.2 | Pipeline for MS patients

For MS patients, T1-weighted MRI were preprocessed as for HC. In addition, the FLAIR images were processed using denoising (Manjón et al., 2010), inhomogeneity correction (Tustison et al., 2010), rigid registration into the T1-weighted MRI native space and then projection into Montreal Neurological Institute (MNI) space using T1-weighted registration matrix. Afterward, MS lesions were segmented using DeepLesionBrain (Kamraoui et al., 2022). This method has been intensively validated on several datasets including different acquisition protocols and scanners. The lesion masks were then used to perform in-painting of MS lesions on T1-weighted MRI (Manjón et al., 2020b). This step was done to limit the impact of MS lesions visible in T1-weighted MRI on brain segmentation. As for HC, at the end, the preprocessed images were controlled using automatic QC (Denis de Senneville et al., 2020) and segmented using AssemblyNet (Coupé et al., 2020b).

In the following, we considered 124 structures of the 132 structures produced by AssemblyNet according to the Neuromorphometrics protocol. First, we used 120 symmetric structures (60 left and 60 right): 9 subcortical structures, 17 frontal gyri/lobules, 8 temporal gyri/lobules, 6 parietal gyri/lobules, 8 occipital gyri/lobules, 6 gyri in the limbic cortex, 5 sub-regions of the insular cortex and the cerebellar GM. Moreover, we used four central structures: the brainstem and three groups of vermal cerebellum lobules (i.e., lobules I–V, lobules VI–VII and lobules VIII–X).

2.5 | Lifespan trajectory estimation

As in (Planche et al., 2022), we used normalized volumes (% of total intracranial volume) to compensate for the head size. Afterward, we used a z-score normalization to enable comparison between structures of different sizes. For each structure, the mean and the standard deviation of the volumes over the HC were used to normalize all the volumes (i.e., both normal and pathological).

Moreover, as in (Coupé et al., 2019), we considered different model types to estimate the best trajectory of each brain structure. To this end, we first estimated several low-order polynomial models (i.e., linear model, quadratic model, and cubic model). In addition, for each structure, we compensated volumes for sex difference using linear model when significant sex effect was detected ($p < .05$) (see Supp. Figure 2 for impact analysis of this correction). Then, we kept a model as a potential candidate when F-statistic based on ANOVA (i.e., model vs. constant model) was significant ($p < .05$) and all its coefficients were significant using t-statistic ($p < .05$). We finally used the Bayesian Information Criterion (BIC) to select the best candidate.

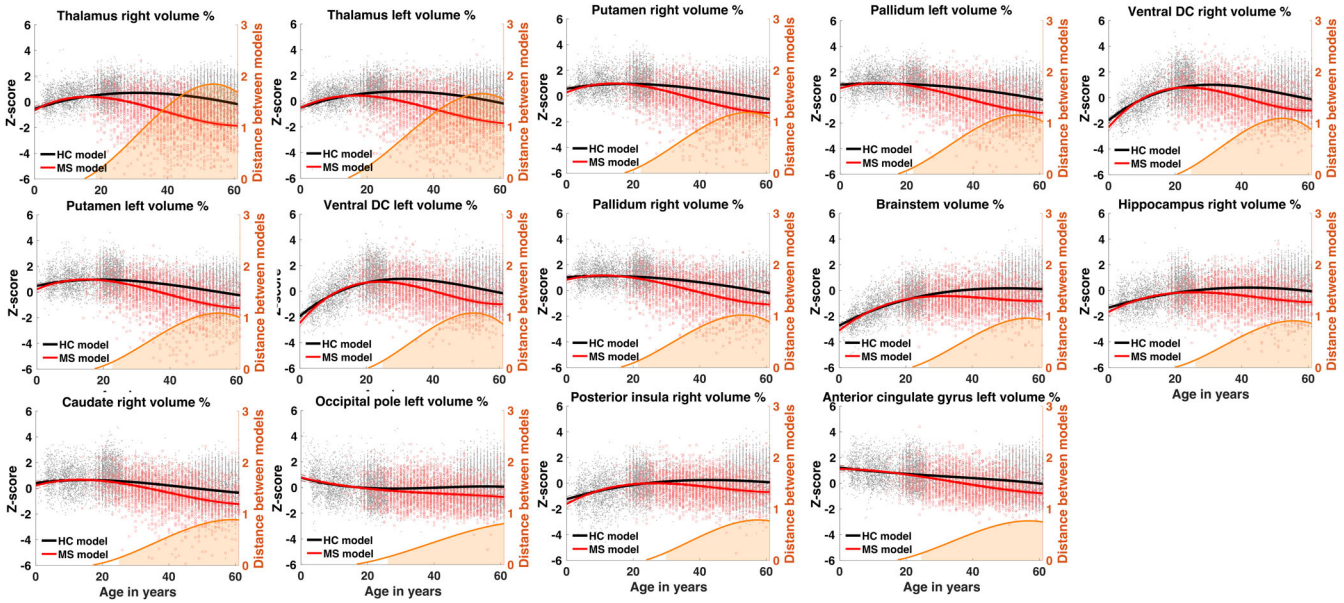

FIGURE 1 Lifespan trajectories based on z-scores of the main impacted brain structures for healthy aging subjects (in black) and MS patients (in red). Black dots represent all healthy individuals and red dots MS patients. The orange curves represent the distance between the healthy and pathological models. The orange areas indicate the time period where confidence intervals of both models do not overlap. The prediction bounds of the models are estimated with an adjusted confidence level at 95%.

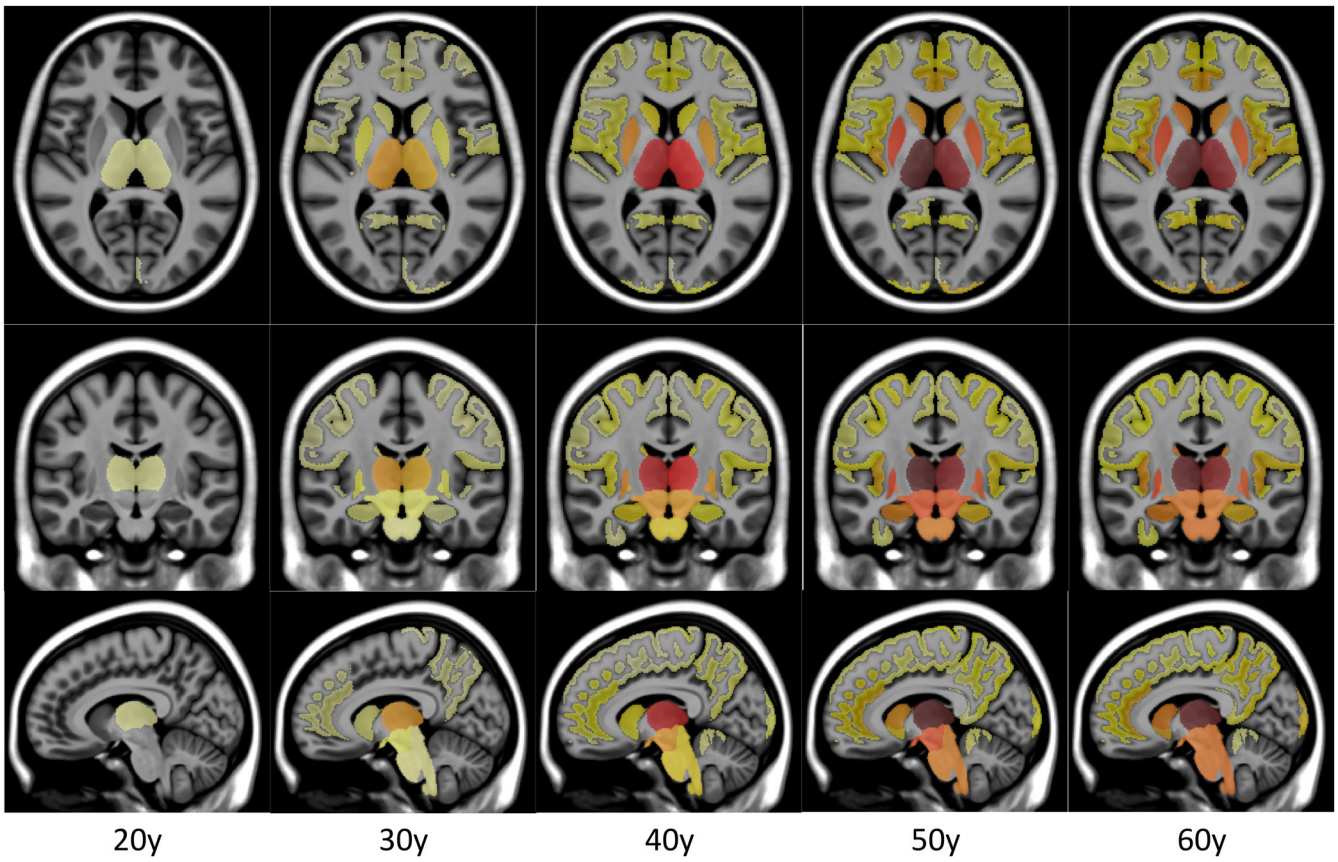

FIGURE 2 Spatiotemporal progression of the MS-related atrophy. Progression of MS-related atrophy along the three axes with radiological convention for all the structures (see Figure S1 for the complete list).

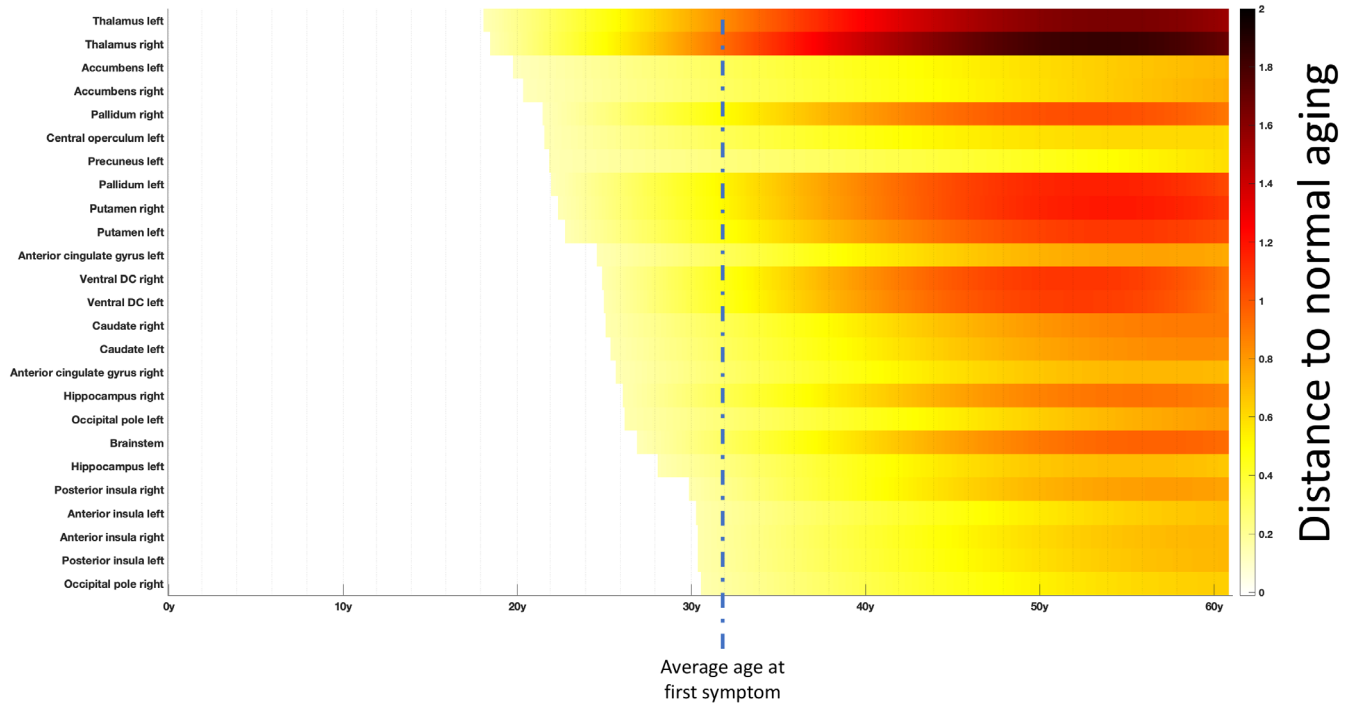

FIGURE 3 Chronological progression of MS over the most impacted structures. Timeline representing the sequential divergence of the most atrophied structures (top 25) between healthy and MS trajectories. The effect-size of structural divergence is color-coded according to the bar at the bottom right of the figure. The mean age at the first symptom (32 years) in this cohort is illustrated with vertical dashed line.

This procedure was done for all the structures and for both populations. All the performed statistics were done using Matlab with default parameters.

2.6 | Divergence between pathological and healthy models

Once the models were estimated for both populations, distances between healthy and MS trajectories were computed for each brain structure. We used an adjusted confidence level of 95% (i.e., 99.96% after correction for multiple comparisons using Dunn's procedure) to estimate the prediction bounds of the trajectories. Moreover, we considered that a structure significantly diverged from normal aging when the adjusted 95% confidence intervals of CN models and MS models do not overlap (Figure 1). Then, all divergent structures were mapped across time and space on the MNI template (see Figure 2). Finally, the sequence of significant divergence of the most affected brain structures (top 25 structures diverging the most) was listed in chronological order to obtain the MRI staging scheme of lifespan MS atrophy (see Figure 3).

3 | RESULTS

First, we compared trajectories of clinical phenotypes of MS. To this end, we estimated the distance between lifespan models of relapsed onset MS (i.e., RRMS+SPMS) and primary progressive MS. We did not find any diverging structures between both groups. Then, we compared trajectories of patients with and without DMT. Similarly, we did not find any diverging structures between both groups. Finally, we compared trajectories patients with MS and HC. We found that 30 left brain structures, 33 right brain structures and 3 central structures (i.e., brainstem, and two groups of cerebellar lobules) significantly diverged between MS patients and normal brain charts (see Figure S1). Therefore, on the 124 studied structures, we found that 66 of them (more than 50%) exhibited significant smaller volumes for MS trajectories.

3.1 | Most impacted structures in terms of atrophy

First, we analyzed the most affected structures over time in terms of atrophy peaks (i.e., maximum z-score difference between HC and MS models). Figure 1 shows models for the most impacted structures. These structures were the right thalamus (1.85 at 54 years), the left thalamus (1.64 at 54 years), the right putamen (1.18 at 54 years), the left pallidum (1.16 at 53 years), the right ventral diencephalon (DC—1.10 at 52 years), the left putamen (1.09 at 55 years), the left ventral DC (1.07 at 52 years), the right pallidum (1.02 at 53 years), the brainstem (0.96 at 57 years), the right hippocampus (0.91 at 56 years), the right caudate (0.89 at 60 years), the left occipital pole (0.79 at 61 years), the right posterior insula (0.78 at 57 years) and left anterior cingulate (0.77 at 57 years).

3.2 | Spatiotemporal evolution of atrophy related to MS

Afterward, we studied the spatiotemporal evolution of the MS patients compared to normal brain charts. To this end, we performed a mapping of the divergence between HC and MS trajectories over an MRI atlas for all the diverging structures (see Figure 2). Moreover, we estimated a global timeline of trajectory divergence considering the top 25 most atrophic structures (see Figure 3).

Thanks to these analyses, we observed that the most pronounced atrophy related to MS started in deep GM structures (mainly thalamus, pallidum and putamen) then spread through the ventral diencephalon (a structure regrouping the hypothalamus, mammillary body, subthalamic nuclei, substantia nigra, red nucleus, lateral geniculate nucleus, and medial geniculate nucleus) to finally reach the brainstem.

The mean age of the most significant atrophy onset was around 18 years for the thalamus, between 22 and 23 years for the pallidum and the putamen, around 25 years for the ventral diencephalon and 27 years for the brainstem. This is to contrast with the mean age of the first symptom that was of 32 years old in our MS cohort. Overall, this means that such lifespan model could help us to estimate atrophy related to MS more than one decade before the first symptom.

Besides, although the divergence was smaller compared with normal aging for cortical atrophy than for deep GM atrophy, we also found cortical atrophy started in the parietal lobe (mainly in the precuneus around 22 years) and the insular cortex (mainly in the central operculum around 22 years) before reaching the limbic cortex (mainly the anterior cingulate gyrus around 25 years) to finally end in the occipital lobe (mainly the occipital pole around 26 years) and the temporal lobe (mainly the hippocampus around 26 years).

4 | DISCUSSION

In this study, we used a massive number of subjects ($N = 40{,}944$) to model the archetype progression of MS-related atrophy at the structure level across the entire lifespan. Thanks to this modeling, we inferred the spatiotemporal sequence of GM atrophy in MS over the entire course of the disease, including the preclinical stage. Moreover, such framework accounted for atrophy due to normal aging since healthy and diseased lifespan models were compared. Thereby, we automatically estimated the most impacted structures, the atrophy evolution and the average age of atrophy onset.

The MRI staging of atrophy involved the thalamus, then the pallidum and putamen, followed by the ventral diencephalon and finally the brainstem. Moreover, we found that the anterior cingulate gyrus, the insular cortex, and the hippocampus were impacted but to a smaller extent. Finally, we observed that the precuneus and the accumbens nuclei, while early impacted, were slightly atrophic compared to the thalamus. Most of these structures have been previously reported as atrophic in the literature (Azevedo et al., 2018; Eshaghi, Marinescu, et al., 2018). The chronological sequence of atrophy reported here is also consistent with a previous study using an event-based analysis (Eshaghi, Marinescu, et al., 2018). Our findings also provide new knowledge that could not have been addressed with these previous studies. Importantly, we estimated the very early divergence in life of normal and pathological brain charts, more than one decade before the average age of symptoms onset (i.e., 32-years-old). This observation echoes the volume loss that was already reported in small sample size cohorts of patient with radiologically and clinically isolated syndrome (Azevedo et al., 2015), but also provides an estimation of the mean age of divergence which has never been reported before. While it is well-known that several white matter lesions are already visible at the time of diagnosis (which is the basis for the MRI-based criteria of dissemination in space and time after a first clinical episode (Thompson et al., 2018)), we also demonstrate here that several GM structures will exhibit atrophy at this time. This argues for a neurodegenerative component that is very early and probably compensated for before that lesions would reach eloquent areas leading to a first clinical episode and, in turn, to the clinical diagnosis (Schoonheim et al., 2022).

The thalamus is the earliest affected structure, which is in line with previous literature pointing out the thalamus as a sensitive MRI biomarker of neurodegeneration in the early stage of MS (Azevedo et al., 2018; Eshaghi, Marinescu, et al., 2018; Ramasamy et al., 2009; Sandi et al., 2021). Thalamic atrophy is correlated with a wide range of clinical manifestations and is an important biomarker of disease progression (Hasan et al., 2011). Significant thalamic atrophy has been found in the early stage of MS suggesting that neurodegeneration begins long before the first symptoms (Eshaghi et al., 2018). However, so far, the dynamic of thalamic atrophy at the preclinical stage of MS was unknown. It is likely that thalamic atrophy and atrophy of the other deep GM nuclei could be altered through several mechanisms explaining their particular vulnerability early in life of the MS patients (Ontaneda et al., 2021). Indeed, it is known that these structures can be altered indirectly through disconnection of their projections by white matter lesions (Kolasinski et al., 2012). Direct targeting might add to this secondary phenomenon and therefore accelerate the overall damages. In this process, the high amount of iron within the deep nuclei (Haider et al., 2014) could accelerate oxidative stress (Zecca et al., 2004). The deep nuclei adjacent to the CSF of the ventricles could also be directly targeted by inflammatory and neurotoxic soluble factors coming from CSF (Bajrami et al., 2022).

On top of the thalamus and the other deep grey matter nuclei, we also found rapid volume loss affecting the brainstem that is directly connected with thalamus and could therefore share the same vulnerability. This also reminds atrophy of the cervical spinal cord that is known to take place rapidly (Biberacher et al., 2015). The cortical ribbon is altered at later stages with some regions showing earlier and more pronounced volume loss than others, especially the hippocampus and the insular cortex. The micro or macrostructural vulnerability of these regions has been continuously highlighted in cross-sectional and short-term longitudinal analyses (Eshaghi, Marinescu, et al., 2018). Their vulnerability could be related to a large number of connections and therefore a higher probability to be affected by white matter disconnections. The CSF flow is also supposed to be more restricted

within the deep invaginations facing these sites which could drive more alterations induced by meningeal inflammation (Haider et al., 2016).

In order to build such average models, we had to make few assumptions. The first is that there is a smooth transition between the normal and pathological states which is the rationale for combining volumes of HC early in life with those from MS patients. This is likely the case regarding (i) the slow rate of atrophy in MS reported before and (ii) the previous validation of our modeling strategy using longitudinal data in other conditions such as Alzheimer's disease (Coupé et al., 2019; Planche et al., 2022). The other assumption is that all the clinical phenotypes of MS follow the same dynamic which is the rationale for combing all of them within a single mean model. To confirm this assumption, we estimated the distance between lifespan models of relapsed MS and primary progressive MS and we did not find any diverging structures between both groups. This result is supported by some histological data showing that the pathological processes are regionally consistent between early relapsing–remitting and progressive MS (Mahad et al., 2015).

During our experiment, we corrected volume for sex effect. As shown in supplementary material (see Figure S2), this correction marginally changed the obtained results. Due to partial and non-harmonized information about imaging protocol over databases, we were not able to correct for scanner type that can be considered as a limitation of our study. However, it has been recently shown that scanner type does not have impact on lifespan volume trajectory (Treit et al., 2022). Finally, we also assumed that patients with disease-modifying therapy (DMT) and without DMT had the same dynamic in terms of atrophy compared to normal aging. To confirm this assumption, we estimated the distance between lifespan models of MS patients with and without DMT and we did not find any diverging structures between both groups. This result is in line with (Eshaghi, Marinescu, et al., 2018).

Overall, the proposed lifespan models could have future potential interests in prognosis and diseased monitoring. We recently showed for Alzheimer's disease that the distance to healthy and diseased lifespan models can be used to detect neurodegenerative pathologies at their earliest stage while taking into account normal aging (Coupé et al., 2022). Therefore, as perspectives, such MS brain charts from high number of data modeling the archetype trajectories are likely to be used for comparing individual patient against the mean dynamic profile, at diagnosis or under therapies.

ACKNOWLEDGMENTS

The C-MIND data used in the preparation of this article were obtained from the C-MIND Data Repository created by the C-MIND study of Normal Brain Development. A listing of the participating sites and a complete listing of the study investigators can be found at https://research.cchmc.org/c-mind. The NDAR data used in the preparation of this manuscript were obtained from the NIH-supported National Database for Autism Research (NDAR). This is supported by the National Institute of Child Health and Human Development, the National Institute on Drug Abuse, the National Institute of Mental Health, and the National Institute of Neurological Disorders and Stroke. A listing of the participating sites and a complete listing of the study investigators can be found at http://pediatricmri.nih.gov/nihpd/info/participating_centers.html. The ICBM data used in the preparation of this manuscript were supported by Human Brain Project Grant PO1MHO52176-11 and Canadian Institutes of Health Research Grant MOP-34996. The IXI data used in the preparation of this manuscript were supported by the UK Engineering and Physical Sciences Research Council (EPSRC) GR/S21533/02 - http://www.brain-development.org/. The ABIDE data used in the preparation of this manuscript were supported by ABIDE funding resources listed at http://fcon_1000.projects.nitrc.org/indi/abide/. The ADNI data used in the preparation of this manuscript were obtained from the Alzheimer's Disease Neuroimaging Initiative (ADNI) (National Institutes of Health Grant U01 AG024904). The ADNI is funded by the National Institute on Aging and the National Institute of Biomedical Imaging and Bioengineering and through generous contributions from private partners as well as nonprofit partners listed at: https://ida.loni.usc.edu/collaboration/access/appLicense.jsp. Private sector contributions to the ADNI are facilitated by the Foundation for the National Institutes of Health (www.fnih.org). The grantee organization is the Northern California Institute for Research and Education, and the study was coordinated by the Alzheimer's Disease Cooperative Study at the University of California, San Diego. ADNI data are disseminated by the Laboratory for NeuroImaging at the University of California, Los Angeles. This research was also supported by NIH grants P30AG010129, K01 AG030514 and the Dana Foundation. The AIBL data used in the preparation of this manuscript were obtained from the AIBL study of ageing funded by the Common-wealth Scientific Industrial Research Organization (CSIRO; a publicly funded government research organization), Science Industry Endowment Fund, National Health and Medical Research Council of Australia (Project Grant 1011689), Alzheimer's Association, Alzheimer's Drug Discovery Foundation, and an anonymous foundation. See www.aibl.csiro.au for further details. The ADHAD, DLBS and SALD data used in the preparation of this article were obtained from http://fcon_1000.projects.nitrc.org (Mennes M et al., NeuroImage, 2013; Wei D et al., bioRxiv 2017). The ISYB data were download from https://www.scidb.cn (Imaging Chinese Young Brains, https://doi.org/10.11922/sciencedb.00740). Data used in the preparation of this article were also obtained from the MIRIAD database (Malone IB et al., NeuroImage, 2012) The MIRIAD investigators did not participate in analysis or writing of this report. The MIRIAD dataset is made available through the support of the UK Alzheimer's Society (Grant RF116). The original data collection was funded through an unrestricted educational grant from GlaxoSmithKline (Grant 6GKC). Data used in the preparation of this article were obtained from the Parkinson's Progression Markers Initiative (PPMI) database (www.ppmi-info.org). PPMI—a public-private partnership—was funded by The Michael J. Fox Foundation for Parkinson's Research and funding partners that can be found at https://www.ppmi-info.org/about-ppmi/who-we-are/study-sponsors. The Amsterdam open MRI collection AOMIC ID-1000/PIOP1/PIOP2 data used in the preparation of this article were obtained from https://

nilab-uva.github.io/AOMIC.github.io/ (Snoek L et al., Scientific data, 2021). The Calgary preschool MRI dataset was available at https://osf.io/axz5r/ and supported by University of Calgary and CIHR (IHD-134090 & MOP-136797). Data collection and sharing for this project was provided by the Cambridge Centre for Ageing and Neuroscience (CamCAN, https://camcan-archive.mrc-cbu.cam.ac.uk/dataaccess/). CamCAN funding was provided by the UK Biotechnology and Biological Sciences Research Council (Grant number BB/H008217/1), together with support from the UK Medical Research Council and University of Cambridge, UK. The Pixar database and related fundings were available at https://openneuro.org/datasets/ds000228/versions/1.1.0 (Richardson H et al., Nat Commun, 2018). Data used in the preparation of this work were obtained from the DecNef Project Brain Data Repository (https://bicr-resource.atr.jp/srpbsopen/) gathered by a consortium as part of the Japanese Strategic Research Program for the Promotion of Brain Science (SRPBS) supported by the Japanese Advanced Research and Development Programs for Medical Innovation (AMED, Tanaka SC et al., Scientific data, 2021). FTLDNI was funded through the National Institute of Aging, and started in 2010. The primary goals of FTLDNI were to identify neuroimaging modalities and methods of analysis for tracking frontotemporal lobar degeneration (FTLD) and to assess the value of imaging versus other biomarkers in diagnostic roles. The Principal Investigator of NIFD was Dr. Howard Rosen, MD at the University of California, San Francisco. The data are the result of collaborative efforts at three sites in North America. For up-to-date information on participation and protocol, please visit http://memory.ucsf.edu/research/studies/nifd. Data collection and sharing for this project was funded by the Frontotemporal Lobar Degeneration Neuroimaging Initiative (National Institutes of Health Grant R01 AG032306). The study is coordinated through the University of California, San Francisco, Memory and Aging Center. FTLDNI data are disseminated by the Laboratory for Neuro Imaging at the University of Southern California. The NACC database was funded by NIA/NIH Grants listed at https://naccdata.org/publish-project/authors-checklist#acknowledgment. This research has been conducted using the UK Biobank Resource under application number 80509. See https://www.ukbiobank.ac.uk/ for further details. Data collection has been supported by a grant provided by the French State and handled by the "Agence Nationale de la Recherche," within the framework of the "Investments for the Future" programme, under the reference ANR-10-COHO-002, Observatoire Français de la Sclérose en Plaques (OFSEP)" & "Eugène Devic EDMUS Foundation against multiple sclerosis." We wish to thank all investigators of these projects who collected these datasets and made them freely accessible. This manuscript reflects the views of the authors and may not reflect the opinions or views of the database providers.

FUNDING INFORMATION

This work benefited from the support of the project DeepvolBrain of the French National Research Agency (ANR-18-CE45-0013). This study was achieved within the context of the Laboratory of Excellence TRAIL ANR-10-LABX-57 for the BigDataBrain project. Moreover, we thank the Investments for the future Program IdEx Bordeaux (ANR-10-IDEX-03-02 and RRI "IMPACT"), the French Ministry of Education and Research, and the CNRS for DeepMultiBrain project. This study has also been supported by the PID2020-118608RB-I00 grant from the Spanish Ministerio de Ciencia e Innovación.

CONFLICT OF INTEREST STATEMENT

The authors declare no competing financial interests relative to the present study.

DATA AVAILABILITY STATEMENT

The data that support the findings of this study are available from OFSEP. Restrictions apply to the availability of these data, which were used under license for this study. Data are available from https://www.ofsep.org/fr/ with the permission of OFSEP.

ORCID

Pierrick Coupé https://orcid.org/0000-0003-2709-3350
Ismail Koubiyr https://orcid.org/0000-0001-7185-7974

REFERENCES

Amato, M. P., Bartolozzi, M. L., Zipoli, V., Portaccio, E., Mortilla, M., Guidi, L., Siracusa, G., Sorbi, S., Federico, A., & de Stefano, N. (2004). Neocortical volume decrease in relapsing–remitting MS patients with mild cognitive impairment. *Neurology*, *63*, 89–93.

Avants, B. B., Tustison, N. J., Song, G., Cook, P. A., Klein, A., & Gee, J. C. (2011). A reproducible evaluation of ANTs similarity metric performance in brain image registration. *NeuroImage*, *54*, 2033–2044. https://doi.org/10.1016/j.neuroimage.2010.09.025

Azevedo, C. J., Cen, S. Y., Khadka, S., Liu, S., Kornak, J., Shi, Y., Zheng, L., Hauser, S. L., & Pelletier, D. (2018). Thalamic atrophy in multiple sclerosis: A magnetic resonance imaging marker of neurodegeneration throughout disease. *Annals of Neurology*, *83*, 223–234.

Azevedo, C. J., Overton, E., Khadka, S., Buckley, J., Liu, S., Sampat, M., Kantarci, O., Lebrun Frenay, C., Siva, A., Okuda, D. T., & Pelletier, D. (2015). Early CNS neurodegeneration in radiologically isolated syndrome. *Neurology-Neuroimmunology Neuroinflammation*, *2*, 2.

Bajrami, A., Magliozzi, R., Pisani, A. I., Pizzini, F. B., Crescenzo, F., Marastoni, D., & Calabrese, M. (2022). Volume changes of thalamus, hippocampus and cerebellum are associated with specific CSF profile in MS. *Multiple Sclerosis Journal*, *28*, 550–560.

Biberacher, V., Boucard, C. C., Schmidt, P., Engl, C., Buck, D., Berthele, A., Hoshi, M. M., Zimmer, C., Hemmer, B., & Mühlau, M. (2015). Atrophy and structural variability of the upper cervical cord in early multiple sclerosis. *Multiple Sclerosis Journal*, *21*, 875–884.

Coupé, P., Catheline, G., Lanuza, E., Manjón, J. V., & for the Alzheimer's Disease Neuroimaging Initiative. (2017). Towards a unified analysis of brain maturation and aging across the entire lifespan: A MRI analysis: Towards a unified analysis of brain. *Human Brain Mapping*, *38*, 5501–5518. https://doi.org/10.1002/hbm.23743

Coupé, P., Manjón, J. V., Lanuza, E., & Catheline, G. (2019). Lifespan changes of the human brain in Alzheimer's disease. *Scientific Reports*, *9*, 3998. https://doi.org/10.1038/s41598-019-39809-8

Coupé, P., Manjón, J. V., Mansencal, B., Tourdias, T., Catheline, G., & Planche, V. (2022). Hippocampal-amygdalo-ventricular atrophy score: Alzheimer disease detection using normative and pathological lifespan models. *Human Brain Mapping*, *43*, 3270–3282.

Coupé, P., Mansencal, B., Clément, M., Giraud, R., de Denis, Senneville, B., Ta, V. T., Lepetit, V., & Manjon, J. V. (2020a). AssemblyNet: A large ensemble of CNNs for 3D whole brain MRI segmentation. *NeuroImage*, *219*, 117026. https://doi.org/10.1016/j.neuroimage.2020.117026

Dalton, C. M., Chard, D. T., Davies, G. R., Miszkiel, K. A., Altmann, D. R., Fernando, K., Plant, G. T., Thompson, A. J., & Miller, D. H. (2004). Early development of multiple sclerosis is associated with progressive grey matter atrophy in patients presenting with clinically isolated syndromes. *Brain*, *127*, 1101–1107.

de Denis, Senneville, B., Manjón, J. V., & Coupé, P. (2020). RegQCNET: Deep quality control for image-to-template brain MRI affine registration. *Physics in Medicine and Biology*, *65*, 225022. https://doi.org/10.1088/1361-6560/abb6be

Eshaghi, A., Marinescu, R. V., Young, A. L., Firth, N. C., Prados, F., Jorge Cardoso, M., Tur, C., de Angelis, F., Cawley, N., Brownlee, W. J., de Stefano, N., Laura Stromillo, M., Battaglini, M., Ruggieri, S., Gasperini, C., Filippi, M., Rocca, M. A., Rovira, A., Sastre-Garriga, J., … Ciccarelli, O. (2018). Progression of regional grey matter atrophy in multiple sclerosis. *Brain*, *141*, 1665–1677.

Eshaghi, A., Prados, F., Brownlee, W. J., Altmann, D. R., Tur, C., Cardoso, M. J., de Angelis, F., van de Pavert, S. H., Cawley, N., de Stefano, N., Stromillo, M. L., Battaglini, M., Ruggieri, S., Gasperini, C., Filippi, M., Rocca, M. A., Rovira, A., Sastre-Garriga, J., Vrenken, H., … MAGNIMS Study Group. (2018). Deep gray matter volume loss drives disability worsening in multiple sclerosis. *Annals of Neurology*, *83*, 210–222.

Filippi, M., Preziosa, P., Copetti, M., Riccitelli, G., Horsfield, M. A., Martinelli, V., Comi, G., & Rocca, M. A. (2013). Gray matter damage predicts the accumulation of disability 13 years later in MS. *Neurology*, *81*, 1759–1767.

Fisher, E., Lee, J.-C., Nakamura, K., & Rudick, R. A. (2008). Gray matter atrophy in multiple sclerosis: A longitudinal study. *Annals of Neurology: Official Journal of the American Neurological Association and the Child Neurology Society*, *64*, 255–265.

Haider, L., Simeonidou, C., Steinberger, G., Hametner, S., Grigoriadis, N., Deretzi, G., Kovacs, G. G., Kutzelnigg, A., Lassmann, H., & Frischer, J. M. (2014). Multiple sclerosis deep grey matter: The relation between demyelination, neurodegeneration, inflammation and iron. *Journal of Neurology, Neurosurgery & Psychiatry*, *85*, 1386–1395.

Haider, L., Zrzavy, T., Hametner, S., Höftberger, R., Bagnato, F., Grabner, G., Trattnig, S., Pfeifenbring, S., Brück, W., & Lassmann, H. (2016). The topograpy of demyelination and neurodegeneration in the multiple sclerosis brain. *Brain*, *139*, 807–815.

Hasan, K. M., Walimuni, I. S., Abid, H., Frye, R. E., Ewing-Cobbs, L., Wolinsky, J. S., & Narayana, P. A. (2011). Multimodal quantitative magnetic resonance imaging of thalamic development and aging across the human lifespan: Implications to neurodegeneration in multiple sclerosis. *Journal of Neuroscience*, *31*, 16826–16832.

Henry, R. G., Shieh, M., Okuda, D. T., Evangelista, A., Gorno-Tempini, M. L., & Pelletier, D. (2008). Regional grey matter atrophy in clinically isolated syndromes at presentation. *Journal of Neurology, Neurosurgery & Psychiatry*, *79*, 1236–1244.

Kamraoui, R. A., Ta, V.-T., Tourdias, T., Mansencal, B., Manjon, J. V., & Coup, P. (2022). DeepLesionBrain: Towards a broader deep-learning generalization for multiple sclerosis lesion segmentation. *Medical Image Analysis*, *76*, 102312.

Kolasinski, J., Stagg, C. J., Chance, S. A., DeLuca, G. C., Esiri, M. M., Chang, E. H., Palace, J. A., McNab, J. A., Jenkinson, M., Miller, K. L., & Johansen-Berg, H. (2012). A combined post-mortem magnetic resonance imaging and quantitative histological study of multiple sclerosis pathology. *Brain*, *135*, 2938–2951.

Labiano-Fontcuberta, A., Mato-Abad, V., Álvarez-Linera, J., Hernández-Tamames, J. A., Martínez-Ginés, M. L., Aladro, Y., Ayuso, L., Domingo-Santos, Á., & Benito-León, J. (2016). Gray matter involvement in radiologically isolated syndrome. *Medicine*, *95*, e3208.

Mahad, D. H., Trapp, B. D., & Lassmann, H. (2015). Pathological mechanisms in progressive multiple sclerosis. *The Lancet Neurology*, *14*, 183–193.

Manjón, J. V., Romero, J. E., Vivo-Hernando, R., Gregorio, R. N., de la María, I. V., Fernando, A. R., & Pierrick, C. (2020a). Deep ICE: A deep learning approach for MRI intracranial cavity extraction. https://doi.org/10.48550/arXiv.2001.05720

Manjón, J. V., Romero, J. E., Vivo-Hernando, R., Rubio, G., Aparici, F., de la Iglesia-Vaya, M., Tourdias, T., & Coupé, P. (2020b). Blind MRI brain lesion inpainting using deep learning. In *International workshop on simulation and synthesis in medical imaging* (pp. 41–49). Springer.

Manjón, J. V., Tohka, J., García-Martí, G., Carbonell-Caballero, J., Lull, J. J., Martí-Bonmatí, L., & Robles, M. (2008). Robust MRI brain tissue parameter estimation by multistage outlier rejection. *Magnetic Resonance in Medicine*, *59*, 866–873. https://doi.org/10.1002/mrm.21521

Manjón, J. V., Tohka, J., & Robles, M. (2010). Improved estimates of partial volume coefficients from noisy brain MRI using spatial context. *NeuroImage*, *53*, 480–490. https://doi.org/10.1016/j.neuroimage.2010.06.046

Marciniewicz, E., Bladowska, J., Podgórski, P., & Sąsiadek, M. (2019). The role of MR volumetry in brain atrophy assessment in multiple sclerosis: A review of the literature. *Advances in Clinical and Experimental Medicine: Official Organ Wroclaw Medical University*, *28*, 989–999.

Ontaneda, D., Raza, P. C., Mahajan, K. R., Arnold, D. L., Dwyer, M. G., Gauthier, S. A., Greve, D. N., Harrison, D. M., Henry, R. G., Li, D. K. B., Mainero, C., Moore, W., Narayanan, S., Oh, J., Patel, R., Pelletier, D., Rauscher, A., Rooney, W. D., Sicotte, N. L., … the North American Imaging in Multiple Sclerosis Cooperative (NAIMS). (2021). Deep grey matter injury in multiple sclerosis: A NAIMS consensus statement. *Brain*, *144*, 1974–1984.

Planche, V., Manjon, J. V., Mansencal, B., Lanuza, E., Tourdias, T., Catheline, G., & Coupé, P. (2022). Structural progression of Alzheimer's disease over decades: The MRI staging scheme. *Brain Communications*, *4*, fcac109.

Planche, V., Mansencal, B., Manjon, J. V., Tourdias, T., Catheline, G., Coupé, P., & For the Frontotemporal Lobar Degeneration Neuroimaging Initiative and the National Alzheimer's Coordinating Center cohort. (2023). Anatomical MRI staging of frontotemporal dementia variants. *Alzheimer's & Dementia*, alz.12975. https://doi.org/10.1002/alz.12975

Ramasamy, D. P., Benedict, R. H., Cox, J. L., Fritz, D., Abdelrahman, N., Hussein, S., Minagar, A., Dwyer, M. G., & Zivadinov, R. (2009). Extent of cerebellum, subcortical and cortical atrophy in patients with MS: A case-control study. *Journal of the Neurological Sciences*, *282*, 47–54.

Sandi, D., Fricska-Nagy, Z., Bencsik, K., & Vécsei, L. (2021). Neurodegeneration in multiple sclerosis: Symptoms of silent progression, biomarkers and neuroprotective therapy—Kynurenines are important players. *Molecules*, *26*, 3423.

Schoonheim, M. M., Broeders, T. A., & Geurts, J. J. (2022). The network collapse in multiple sclerosis: An overview of novel concepts to address disease dynamics. *NeuroImage: Clinical*, *35*, 103108.

Thompson, A. J., Banwell, B. L., Barkhof, F., Carroll, W. M., Coetzee, T., Comi, G., Correale, J., Fazekas, F., Filippi, M., Freedman, M. S., Fujihara, K., Galetta, S. L., Hartung, H. P., Kappos, L., Lublin, F. D., Marrie, R. A., Miller, A. E., Miller, D. H., Montalban, X., … Cohen, J. A. (2018). Diagnosis of multiple sclerosis: 2017 revisions of the McDonald criteria. *The Lancet Neurology*, *17*, 162–173.

Treit, S., Stolz, E., Rickard, J. N., McCreary, C. R., Bagshawe, M., Frayne, R., Lebel, C., Emery, D., & Beaulieu, C. (2022). Lifespan volume trajectories from non–harmonized T1–weighted MRI do not differ after site correction based on traveling human phantoms. *Frontiers in Neurology*, *13*, 826564.

Tustison, N. J., Avants, B. B., Cook, P. A., Zheng, Y., Egan, A., Yushkevich, P. A., & Gee, J. C. (2010). N4ITK: Improved N3 bias correction. *IEEE Transactions on Medical Imaging*, *29*, 1310–1320.

Vukusic, S., Casey, R., Rollot, F., Brochet, B., Pelletier, J., Laplaud, D. A., de Sèze, J., Cotton, F., Moreau, T., Stankoff, B., Fontaine, B., Guillemin, F., Debouverie, M., & Clanet, M. (2020). Observatoire Français de la Sclérose en Plaques (OFSEP): A unique multimodal nationwide MS registry in France. *Multiple Sclerosis Journal*, *26*, 118–122.

Zecca, L., Youdim, M. B., Riederer, P., Connor, J. R., & Crichton, R. R. (2004). Iron, brain ageing and neurodegenerative disorders. *Nature Reviews Neuroscience*, *5*, 863–873.

SUPPORTING INFORMATION

Additional supporting information can be found online in the Supporting Information section at the end of this article.

How to cite this article: Coupé, P., Planche, V., Mansencal, B., Kamroui, R. A., Koubiyr, I., Manjòn, J. V., & Tourdias, T. (2023). Lifespan neurodegeneration of the human brain in multiple sclerosis. *Human Brain Mapping*, *44*(17), 5602–5611. https://doi.org/10.1002/hbm.26464